minerals

MDPI

Article

Fibrous Platinum-Group Minerals in "Floating Chromitites" from the Loma Larga Ni-Laterite Deposit, Dominican Republic

Thomas Aiglsperger [1,*], Joaquín A. Proenza [1], Francisco Longo [2], Mercè Font-Bardia [1], Salvador Galí [1], Josep Roqué [1] and Sandra Baurier-Aymat [1]

[1] Departament de Mineralogia, Petrologia i Geologia Aplicada, Facultat de Ciències de la Terra, Universitat de Barcelona (UB), Martí i Franquès s/n, Barcelona 08028, Spain; japroenza@ub.edu (J.A.P.); mercef@ccit.ub.edu (M.F.-B.); salvadorgali@gmail.com (S.G.); josep.roque.rosell@gmail.com (J.R.); sandrabaurier@gmail.com (S.B.-A.)

[2] Faculty of Engineering, Universidad Católica Tecnológica del Cibao (UCATECI), Ave. Universitaria, esq. Ave. Pedro Rivera, P.O. Box 401, La Vega, Dominican Republic; longof@claro.net.do

* Correspondence: thomas.aiglsperger@ub.edu; Tel.: +34-93-402-1341

Academic Editor: Maria Economou-Eliopoulos
Received: 8 August 2016; Accepted: 16 November 2016; Published: 30 November 2016

Abstract: This contribution reports on the observation of enigmatic fibrous platinum-group minerals (PGM) found within a chromitite body included in limonite ("floating chromitite") from Ni-laterites in the Dominican Republic. Fibrous PGM have a Ru-Os-Ir-Fe dominated composition and are characterized by fibrous textures explained by grain-forming fibers which are significantly longer (1–5 μm) than they are wide (~100 nm). Back-scattered electron (BSE) images suggest that these nanofibers are platinum-group elements (PGE)-bearing and form <5 μm thick layers of bundles which are oriented orthogonal to grains' surfaces. Trace amounts of Si are most likely associated with PGE-bearing nanofibers. One characteristic fibrous PGM was studied in detail: XRD analyses point to ruthenian hexaferrum. However, the unpolished fibrous PGM shows numerous complex textures on its surface which are suggestive for neoformation processes: (i) features suggesting growth of PGE-bearing nanofibers; (ii) occurrence of PGM nanoparticles within film material (biofilm?) associated with PGE-bearing nanofibers; (iii) a Si-rich and crater-like texture hosting PGM nanoparticles and an Ir-rich accumulation of irregular shape; (iv) complex PGM nanoparticles with ragged morphologies, resembling sponge spicules and (v) oval forms (<1 μm in diameter) with included PGM nanoparticles, similar to those observed in experiments with PGE-reducing bacteria. Fibrous PGM found in the limonite may have formed due to supergene (bio-)weathering of fibrous Mg-silicates which were incorporated into desulphurized laurite during stages of serpentinization.

Keywords: PGE; PGM; fibrous; nanofibers; Ni-laterite; supergene; weathering; neoformation; Falcondo; Dominican Republic

1. Introduction

The platinum-group elements (PGE) are a group of precious metals (Os, Ir, Ru, Rh, Pt, and Pd) which are referred to strategic metals because of their extreme scarcity within the Earth's crust combined with the increasing need for PGE in advanced technologies (e.g., autocatalyst industries; electronics) and jewellery [1]. Currently, the vast majority (~80%) of the worldwide PGE demand is supplied by magmatic ore deposits located in only two countries, i.e., South Africa and Russia [2]. This supply situation has motivated the search for alternative sources of PGE, and large oxidized ore deposits associated with near surface modification of ultramafic rocks, such as ophiolite-related Ni-laterites, have been considered as worthy exploration targets for future unconventional PGE ore

deposits [3]. In general, total PGE contents found in Ni-laterites around the world are in the range of <100 ppb to up to a few hundred ppb, however lateritic crust with 2 ppm PGE was reported from Western Australia [4] as well as >4 ppm PGE from Burundi [5].

Ni-laterites from the northern Caribbean are systematically enriched in the limonite and reach values of up to 0.6 ppm total PGE [6]. These increasing PGE contents toward the surface are mainly explained by residual accumulations of PGE-bearing minerals. However, the results of detailed mineralogical surveys also provide convincing morphological and chemical evidence for in situ neoformation of platinum-group minerals (PGM) within Ni-laterites by bioreduction and/or electrochemical accretion [7,8]. Hence, accumulations of what are most likely biogenic mediated in situ growths of PGM nanoparticles are believed to contribute to PGE anomalies in Ni-laterites. The recent verification of the biological role of PGM transformations in supergene environments by [9] has marked the beginning of a new period of PGE-related investigation and exploration.

The presented contribution reports on the observation of enigmatic fibrous PGM found close to the surface in Ni-laterites from the Dominican Republic and aims (i) to give a general overview of the prevailing features of fibrous PGM; (ii) to provide detailed textural as well as mineralogical data of one characteristic fibrous PGM and (iii) to discuss a possible origin of fibrous PGM.

2. Sample Material and Methods

Samples were collected in the ophiolite-related Loma Larga Ni-laterite ore deposit which forms part of the Falcondo mining area located in the central part of the Dominican Republic (Figure 1). The Falcondo mining area is currently known as the largest hydrous Mg-silicate type Ni-laterite deposit of the Caribbean, with measured and indicated Ni resources of 67.8 Mt at a grade of 1.5% Ni plus 4.9 Mt at 1.4% Ni inferred [10].

The Ni-laterite at Falcondo developed over the so-called Loma Caribe peridotite which occurs as a serpentinized belt of ultramafic rocks approximately 4–5 km wide and 95 km long in the northwest of Santo Domingo (Figure 1). Detailed information of the local geology and formation history of the Ni-laterites can be found elsewhere (e.g., [11] and references therein). In general, the weathering profile of the Falcondo mining area is divided into: (i) serpentinized protolith (harzburgite > dunite > lherzolite) at the bottom followed by (ii) saprolite with hydrous Mg-silicate dominated mineralogy (beneath the Mg-discontinuity) and (iii) limonite with Fe-oxide(s) dominated mineralogy at the top (above the Mg-discontinuity) [11–14].

Small, rare, and hence uneconomic chromitite occurrences are scattered within given horizons of the lateritic profile [15,16]. Within the Ni-laterite profile of the Loma Larga ore deposit a highly weathered chromitite body of approximately 0.5 m × 0.5 m is included in limonite ("floating chromitite") (Figure 1). This chromitite is characterized by extremely high PGE contents up to 17.5 ppm total PGE [7].

Approximately 100 g of homogenized "floating chromitite" sample was carefully disaggregated, milled, and hand-sieved before being processed by means of hydroseparation (HS) techniques at the HS laboratory in Barcelona, Spain ([8] and reference therein). Heavy mineral concentrates were mounted as loose (unpolished) grains on a metallic cylinder (diameter 2.5 cm) and/or as polished monolayer resin blocks and were subsequently investigated by stereomicroscopy, optical reflected light microscopy, and by scanning electron microscopy (SEM) using a Quanta 200 FEI XTE 325/D8395 (FEI, Hillsboro, OR, USA) as well as a field emission scanning electron microscope (FE-SEM) Jeol JSM-7100 (JEOL, Tokyo, Japan) at the Serveis Científics i Tecnòlogics, University of Barcelona, Spain.

At the same institution, quantitative electron microprobe analyses (EMPA) were obtained with a JEOL JXA-8230 electron microprobe (JEOL, Tokyo, Japan) operating in wavelength-dispersive spectroscopy (WDS) mode with an accelerating voltage of 20 kV, a beam current of 10 nA, and a beam diameter of 1 μm. Pure metals were used as standards for Os, Ir, Ru, Rh, Pt, Pd, Co, and Sb as well as chromite (Al, Fe), periclase (Mg), NiO (Ni), S (S), GaAs (As), and wollastonite (Si). The following interferences RuLβ → RhLα, RhLβ → PdLα, RuLβ → PdLα, and RhLα → PtLα were online-corrected.

The same instrument was used for element distribution maps (WDS mode) with an accelerating voltage of 20 kV and a beam current of 128.8 nA. Maps were collected by beam scanning with dwell times of 60 ms/pixel. For each element, the background map was subtracted from the corresponding peak map.

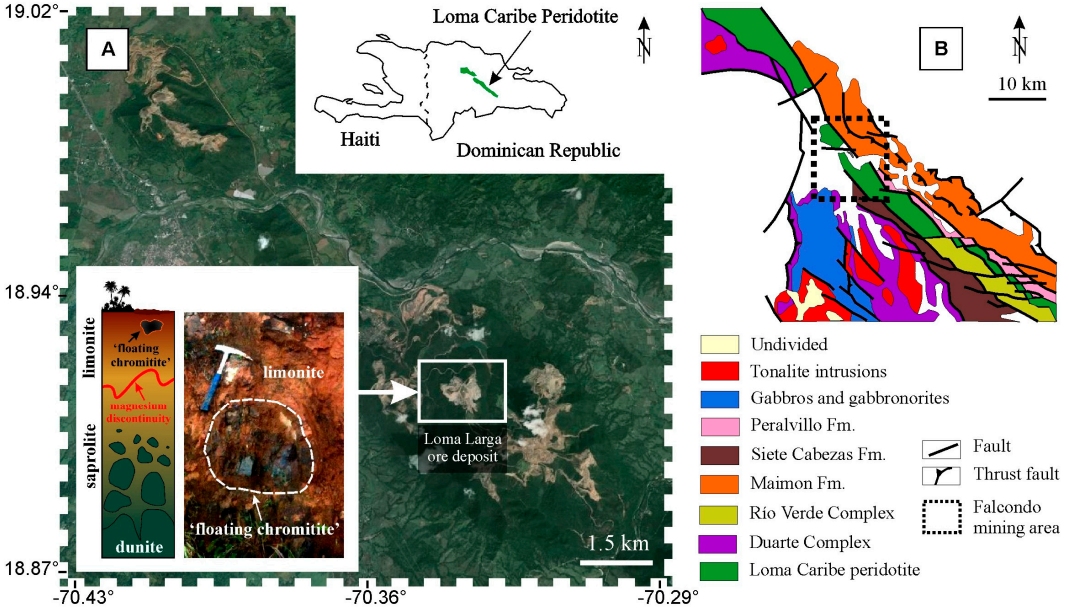

Figure 1. (**A**) The location of the Loma Caribe peridotite and an orthophotograph of the Falcondo mining area highlighting the Loma Larga ore deposit. The inset shows an idealized Ni-laterite soil profile from the Falcondo mining area as well as a field observation of the PGE-rich "floating chromitite" within limonite (width of image: ~1 m); (**B**) Simplified geological map of the central section of the Loma Caribe peridotite (modified from [17,18]).

One fibrous PGM was investigated by single-crystal X-ray diffraction (XRD, Bruker, Billerica, MA, USA) analysis at the same institution. The X-ray intensity data were measured on a D8 Venture system equipped with a multilayer monochromator and a Mo microfocus (λ = 0.71073 Å). The sample was analyzed at a distance of 34 mm. The angles of the goniometer were 2theta = 0°, omega = 360°, and chi = 90°, and the sample was spun 360°. The measuring time was 60 s per step. Subsequent results were processed with Bruker software [19] which was used to subtract the background of the patterns, to detect the peaks, and to assign minerals and their corresponding d_{hkl} to each peak.

3. Mineralogy of Fibrous PGM

Approximately 300 grains of PGM in the size range of <10 µm to ~125 µm in diameter and with either Ru-, Ir-, or Pt-dominated mineralogy were detected in heavy mineral concentrates. Ru-dominated and Fe-rich alloys (e.g., ruthenian hexaferrum) are the most abundant PGM (>90%), followed by lower quantities of Ir- and Pt-bearing Fe-Ni alloys ([7,20] respectively). Careful examination of all PGM via FE-SEM led to the observation of a rarely occurring (~1%), Ru-dominated subgroup which is characterized by fibrous textures (Figure 2). These textures are explained by grain-forming fibers which are significantly longer (1–5 µm) than they are wide (~100 nm). Due to their nanometric diameters, these fibers were defined as nanofibers. In general they occur as <5 µm thick layers of nanofiber-bundles which are oriented orthogonal to the grains' surfaces (Figure 2B,E). Fibrous PGM show diverse morphologies that range from subhedral to anhedral grains (e.g., Figure 2C,I, respectively) and elongated fibrous PGM occur in addition (Figure 2G). Interestingly, some grains contain rounded voids from where nanofiber-bundles propagate radially (Figure 2D,E,I). Energy-dispersive spectroscopy (EDS) analyses (spot diameter of 1 µm) suggest that fibrous PGM contain mainly Ru and Fe with minor contents of Os and Ir. However, small but clear peaks of Si are also observed.

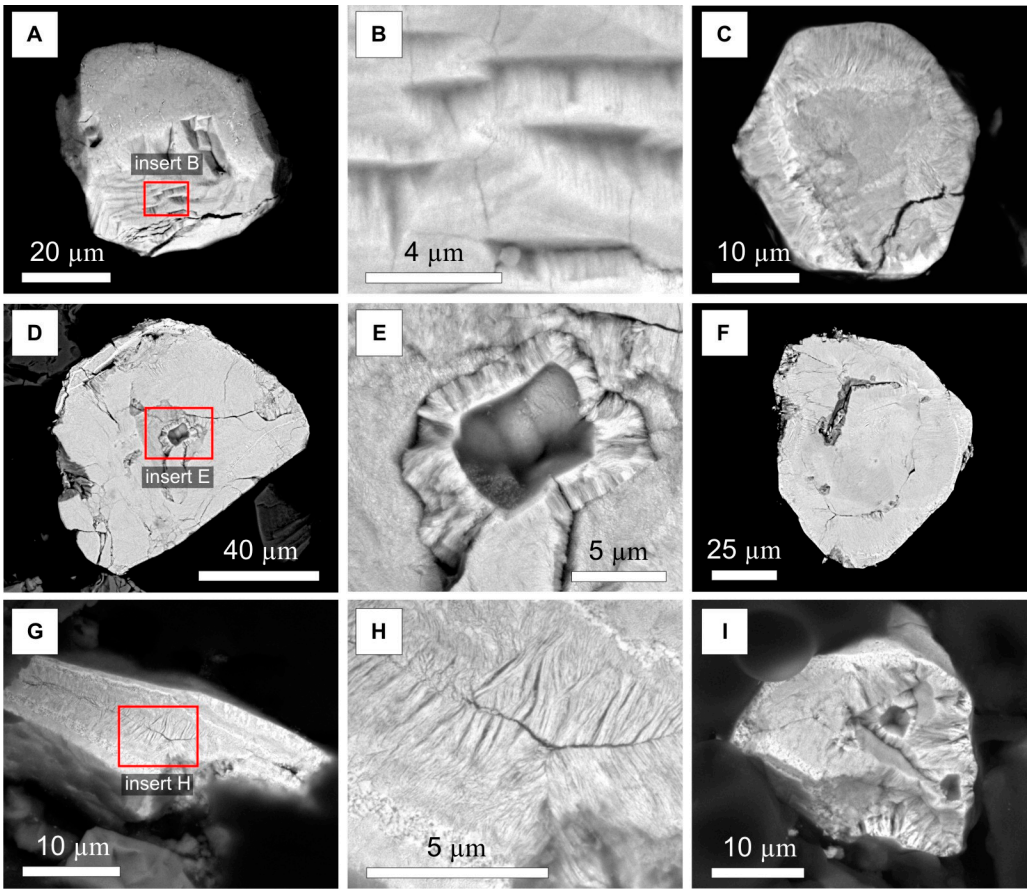

Figure 2. Back-scattered electron (BSE) images of fibrous platinum-group minerals (PGM). (**A**) fibrous PGM with an anhedral shape; note the fractured lower part of the grain revealing numerous layers of nanofiber-bundles; (**B**) close-up of nanofiber-bundles; (**C**) subhedral fibrous PGM; (**D**) anhedral fibrous PGM with a void in its central part; (**E**) close-up showing a void with radially propagating nanofiber-bundles; (**F**) anhedral fibrous PGM; (**G**) fibrous PGM with an elongated morphology; note that nanofiber-bundles have a symmetric distribution and are orthogonal to the surface of the grain; (**H**) close-up showing the central part of an elongated fibrous PGM; (**I**) anhedral fibrous PGM hosting two rounded voids.

3.1. Detailed Investigation of One Fibrous PGM

3.1.1. Field Emission Scanning Electron Microscopy (FE-SEM)

One fibrous PGM was separated and investigated in detail. The unpolished grain has an isometric morphology with approximately 75 µm long axes and is characterized by a subhedral shape with damaged corners and a broken central part (Figure 3A). A detailed survey by means of FE-SEM revealed numerous features on the surface of the grain which, to the best of the authors' knowledge, have not been described for PGM before:

- the structure of the grain suggests an interdependency of PGM nanoparticles and nanofiber-bundles which are oriented orthogonal to the grain's surface (Figure 3A,B,G,H);
- nanofibers occur within layers of nanofiber-bundles as well as within open spaces suggesting either in situ growth ("healing of cracks") or misalignments (Figure 3C,D);
- comparison of BSE images and secondary electron (SE) images suggests that elements of high atomic number (PGE) are present in the central part of the nanofibers (bright in BSE images),

whereas the outer part of the nanofibers appears to consist of elements with lower atomic numbers (e.g., Si) (Figure 3E,F);

- at the endings of nanofiber-bundles, a thin layer of a homogenous film occurs that host PGM nanoparticles (Figure 3G–J);
- within the central part of the grain a Si-rich, crater-like texture is present which occurs dark in BSE images (Figure 3A). This "crater" measures approximately 5 µm × 7 µm in diameter and hosts a great number of homogenously distributed PGM nanoparticles. At its periphery an Ir-rich accumulation (~1 µm in diameter) with a rather irregular shape is observed (Figure 3K);
- around the crater-like texture, PGM nanoparticles occur, which are characterized by ragged morphologies resembling sponge spicules. Interestingly, the Si-rich crater-like texture hosts smaller PGM nanoparticles than its Si-depleted immediate vicinity (Figure 3K);
- on plain walls at the upper part of the grain (Figure 3A), which represent the backside of nanofiber-bundles and therefore most likely film material, oval forms (~500 nm at the long axes) with included PGM nanoparticles occur, resembling observations by [21] in experiments with PGE reducing bacteria (Figure 3L).

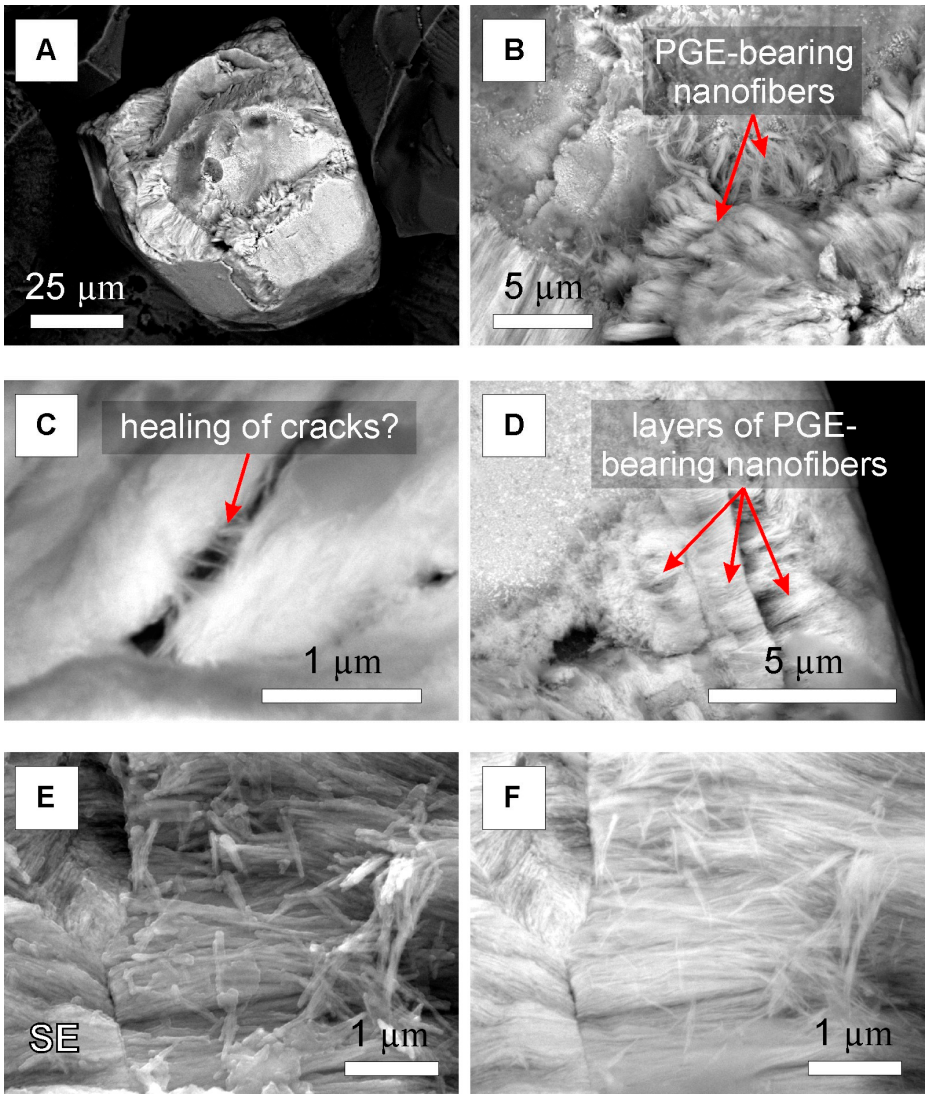

Figure 3. *Cont.*

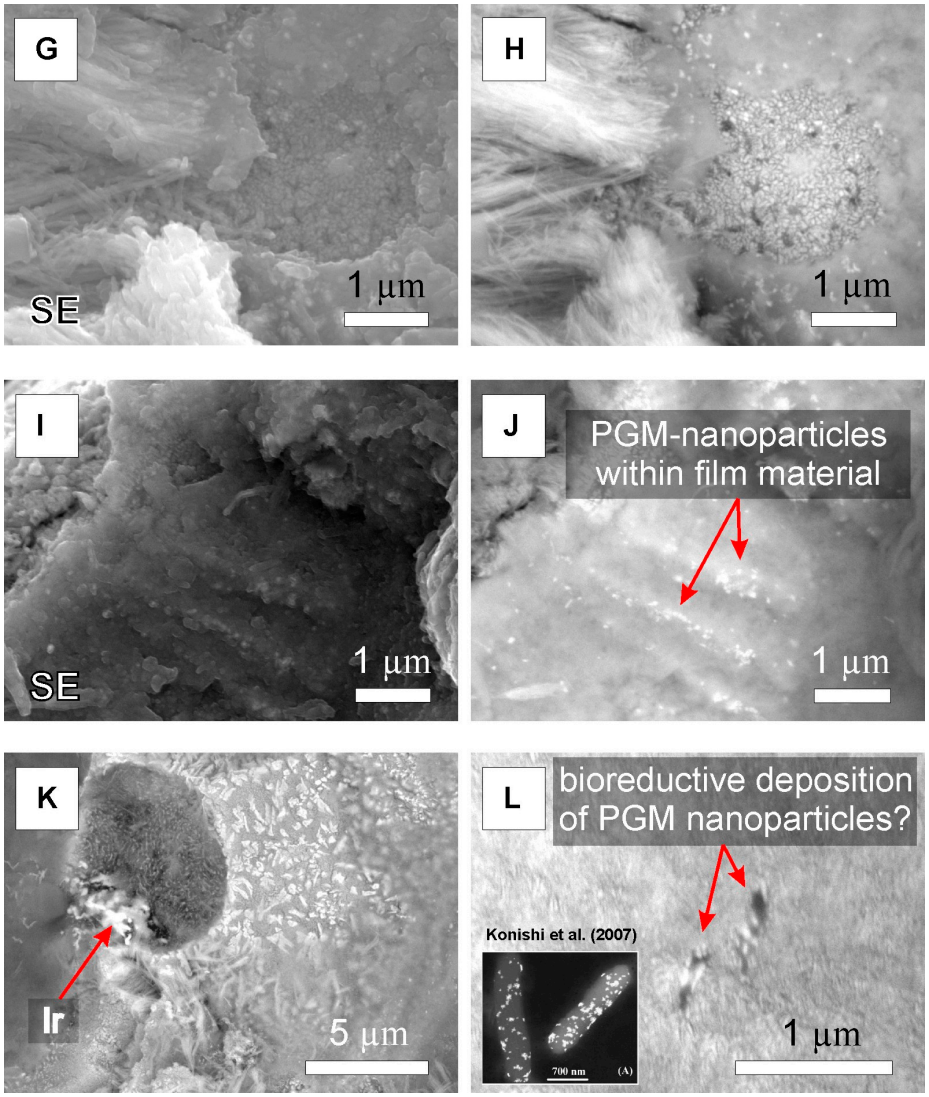

Figure 3. BSE and secondary electron images (SE) of a fibrous PGM showing numerous features: (**A**) overview; note the isometric, subhedral shape of the grain; (**B**) close-up of the platinum-group elements (PGE)-bearing nanofiber-bundles; (**C**) features suggesting either "healing of cracks" or misalignments of nanofibers; (**D**) layers of PGE-bearing nanofiber-bundles which are oriented orthogonal to the grain's surface; (**E**) SE image close-up of nanofibers; (**F**) BSE image close-up of the same area as in (**E**); note the bright occurring center of the nanofibers in the BSE image, suggesting the presence of PGE; (**G**,**H**) close-up of the contact between PGE-bearing nanofiber-bundles and associated film material (biofilm?) hosting PGM nanoparticles in SE (**G**) and BSE (**H**); (**I**,**J**) close-up of the film material showing layering and numerous PGM nanoparticles in SE (**I**) and in BSE (**J**); (**K**) detail of the zone around the crater-like texture in the central part of the grain with associated Ir-rich accumulation and complex morphologies of PGM nanoparticles; note the different size and shape of PGM nanoparticles within the dark (Si-rich) crater-like texture compared to its immediate vicinity; (**L**) approximately 500 nm long oval forms with included PGM nanoparticles resembling observations related to PGE depositing bacteria [21].

3.1.2. X-ray Diffraction (XRD)

The same grain as shown in Figure 3A, revealing metallic luster under the stereomicroscope (Figure 4A), was studied using a single-crystal X-ray diffractometer. The obtained diffraction pattern displayed characteristic concentric, well defined, and homogeneous Debye rings, indicating that the

grain is constituted by a randomly oriented polycrystalline assemblage (Figure 4B). Integration of the intensity data at constant steps of 2θ gives a conventional one dimensional powder diffraction pattern (Figure 4C).

A comparison with literature data for chemically related mineral phases (Os-group minerals) revealed that the fibrous PGM has rather identical X-ray line intensities and observed d-spacings as ruthenian hexaferrum [20] (Table 1). On this basis, the X-ray powder pattern for the fibrous PGM was indexed, leading to the refined unit-cell dimensions: *a* 2.6670 (13) Å, *c* 4.2361 (18) Å, *V*: 26.095 (27) Å^3, *Z* = 2 (Table 2).

Table 1. Powder X-ray data for the fibrous platinum-group mineral (PGM) shown in Figure 3A and comparison with chemically related phases.

Fibrous PGM			**Ruthenian Hexaferrum** [1]			**Hexaferrum (PDF 54-0704)**			**Ruthenium (PDF 00-06-0663)**			**Osmium (PDF 00-041-0601)**		
*I*meas	*d*meas(Å)	*hkl*	*I*meas	*d*meas(Å)	*hkl*	*I*meas	*d*meas(Å)	*hkl*	*I*meas	*d*meas(Å)	*hkl*	*I*meas	*d*meas(Å)	*hkl*
20	2.3097	100	20	2.3068	100	50	2.28	100	40	2.343	100	80	2.363	100
25	2.1181	002	20	2.1250	002	60	2.10	002	35	2.142	002	30	2.166	002
100	2.0279	101	100	2.0274	101	100	2.006	101	100	2.056	101	100	2.071	101
30	1.5611	102	25	1.5629	102	30	1.549	102	25	1.5808	102	40	1.594	102
35	1.3335	110	40	1.3318	110	30	1.316	110	25	1.3530	110	60	1.364	110
40	1.2047	103	50	1.2072	103	30	1.195	103	25	1.2189	103	20	1.232	103
			10	1.1534	200				6	1.1715	200	10	1.180	200
50	1.1285	112	60	1.1285	112	20	1.118	112	25	1.1434	112	50	1.153	112
35	1.1142	201	40	1.1131	201	20	1.108	201	20	1.1299	201	40	1.039	201
									4	1.0705	004	1	1.080	004
									5	1.0278	202	10	1.035	202
									6	0.9738	104	5	0.9835	104
									16	0.9056	203	40	0.9135	203
									6	0.8857	210	10	0.8929	210
									25	0.8673	211	50	0.8737	211
									18	0.8395	114	20	0.8472	114
									10	0.8185	212	20	0.8252	212
									16	0.8043	105	20	0.8123	105
												5	0.7974	204
												10	0.7866	300

[1] [20].

Table 2. Comparative data for chemically related phases including the fibrous PGM.

	Fibrous PGM	**Ruthenian hexaferrum** [1]	**Hexaferrum** [2]	**Ruthenium** [3]	**Osmium** [4]	**Garutiite** [5]
Chem. Formula	(Ru,Os,Ir,Fe,Si,Al,Mn)	$Ru_{0.4}(Os,Ir)_{0.1}Fe_{0.5}$	(Fe,Os,Ru,Ir)	(Ru,Ir,Os)	(Os,Ir,Ru)	(Ni,Fe,Ir)
Crystal System	Hexagonal	Hexagonal	Hexagonal	Hexagonal	Hexagonal	Hexagonal
Group Unit cell	$P6_3/mmc$	$P6_3/mmc$	$P6_3/mmc$	$P6_3/mmc$	$P6_3/mmc$	$P6_3/mmc$
a	2.6670 (13)	2.664 (1)	2.64 (1)	2726	2726	2.6939 (5)
c (Å)	4.2361 (18)	4.250 (2)	4.20 (2)	4326	4326	4.2732 (6)
V (Å^3)	26.095 (27)	26.12 (3)	25.35	27.84	27.84	26.86 (1)
Z	2	2	2	2	2	2

[1] [20]; [2] [22]; [3] [23]; [4] [24]; [5] [25].

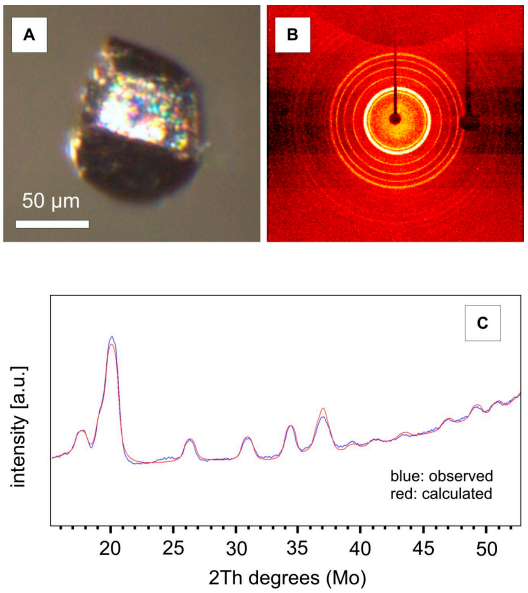

Figure 4. (**A**) Stereomicroscope image of the unpolished fibrous PGM grain showing metallic luster; (**B**) Debye rings for the fibrous PGM, observed on the two dimensional detector; (**C**) Rietveld refinement of the obtained one dimensional conventional diffractogram [19] and the resulting XRD pattern for the fibrous PGM (observed and calculated).

3.1.3. Electron Microprobe Analysis (EMPA)

In continuation, the same grain as shown in Figure 3A was included in epoxy and polished for quantitative analyses as well as for element mappings. Polishing of the fibrous PGM led to a general loss of textures, providing evidence that observed complex textures occur exclusively associated with the surface of fibrous PGM. BSE images of the polished fibrous PGM reveal rather homogenous and bright zones, which are crosscut by a slightly darker, Si-bearing belt of varying thickness (Figure 5A). A close-up image of the Si-bearing belt displays the presence of PGE-bearing nanofibers (Figure 5B).

EMP analyses of four points (indicated in Figure 5A) are given in Table 3 and confirm the dominance of Ru, Os, Fe, and Ir relative to other elements including trace amounts (<1 wt %) of Mn, Si, Al, and Ni. Low totals (<85.55 wt %) are mainly attributed to the fine-grained nature of the grain and maybe also to the possible occurrence of O or OH within the nanofibers. Element mappings of the area indicated in Figure 5A confirm the above-mentioned dominance of Fe-rich, Ru-Os-Ir compositions (Figure 5C). However, within the Si-rich area, lower Fe and Ni contents are observed, Os reveals an elongated zone of slightly higher contents, whereas Ru does not show visible compositional variations (Figure 5C).

Table 3. Composition of the fibrous PGM analyzed by electron microprobe (EMP).

	wt %																	
	S	**As**	**Os**	**Ir**	**Ru**	**Rh**	**Pt**	**Pd**	**Fe**	**Ni**	**Cu**	**Co**	**Si**	**Al**	**Mg**	**Sb**	**Mn**	**Total**
1	0.04	0.15	17.95	5.32	42.96	bdl	bdl	bdl	16.64	0.33	0.09	0.13	0.54	0.62	0.05	bdl	0.59	85.54
2	0.12	0.15	17.78	5.04	40.94	0.12	bdl	bdl	11.36	0.17	0.09	0.07	0.82	0.44	0.03	0.15	0.86	78.14
3	0.06	0.10	16.34	7.78	43.03	bdl	bdl	bdl	14.59	0.29	0.06	0.14	0.47	0.59	0.06	bdl	0.76	84.29
4	0.03	0.09	17.31	7.81	41.56	bdl	bdl	bdl	16.50	0.36	0.10	0.10	0.47	0.60	0.04	bdl	0.58	85.55
	at %																	
	S	**As**	**Os**	**Ir**	**Ru**	**Rh**	**Pt**	**Pd**	**Fe**	**Ni**	**Cu**	**Co**	**Si**	**Al**	**Mg**	**Sb**	**Mn**	
1	0.14	0.22	10.33	3.03	46.54	0.00	0.00	0.00	32.63	0.62	0.16	0.25	2.11	2.50	0.23	0.00	1.17	
2	0.47	0.25	11.62	3.26	50.35	0.14	0.00	0.00	25.29	0.35	0.18	0.15	3.63	2.05	0.16	0.15	1.94	
3	0.20	0.15	9.76	4.60	48.38	0.00	0.00	0.00	29.69	0.56	0.10	0.28	1.92	2.49	0.29	0.00	1.57	
4	0.10	0.13	10.10	4.51	45.63	0.00	0.00	0.00	32.79	0.69	0.17	0.18	1.85	2.48	0.19	0.00	1.18	

bdl = below detection limit.

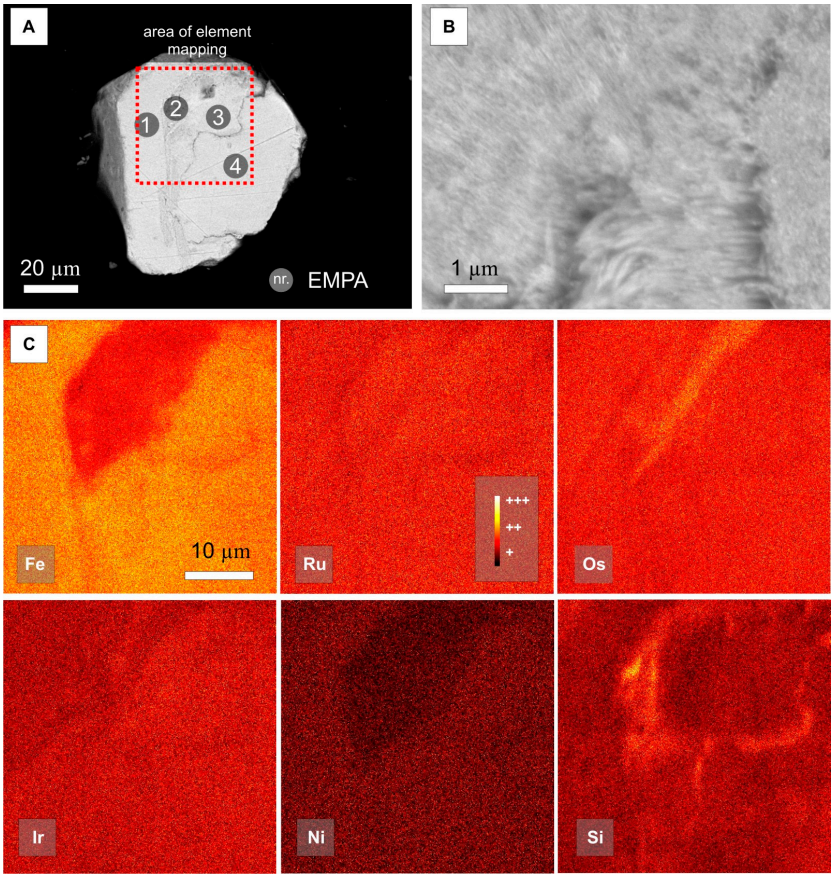

Figure 5. (**A**) BSE image of the polished fibrous PGM shown in Figure 3A with an indicated area of element mapping and points of EMP analyses (EMPA); (**B**) close-up of polished PGE-bearing nanofibers next to EMPA point 2; (**C**) element mapping; note the elevated Si contents where nanofibers are present. For details see the main text.

4. Discussion

The nature and origin of fibrous PGM found in the Loma Larga ore deposit are enigmatic. Radial-fibrous internal textures of secondary PGM derived from the in situ alteration of magmatic laurite at low temperatures were reported from ophiolite-related chromitite samples from Greece [26], and similar secondary grains were also described by [27] from Turkish ophiolites. The latter authors demonstrated that dark zones in BSE images contain significant contents of Si and Mg (up to 9 and 10 at %, respectively), which accounted for sub-microscopic particles of chlorite or serpentine. Such secondary PGM grains with intimate intergrowths of Mg-silicates, believed to form during stages of serpentinization, occur in the study area ([8] and reference therein).

Recent studies have suggested that these Mg-silicates are not stable at higher levels of the Ni-laterite profile (close to the Mg-discontinuity) and are replaced by secondary Fe oxide(s) [20]. The observation of subsequent Fe-incorporation into secondary Ru-Os-Ir alloys via abiotic and/or biological processes has been used as an evidence for a supergene origin of ruthenian hexaferrum found in Ni-laterites from the Dominican Republic [20]. Here, the presented XRD data of one characteristic fibrous PGM with an isometric morphology suggest that such a PGM transformation from primary laurite toward ruthenian hexaferrum has occurred (Figure 3A; Tables 1 and 2). However, PGE-bearing nanofibers have not been observed in ruthenian hexaferrum grains from the study area before.

Complex textures such as PGM nanoparticles within film material (Figure 3I,J), as well as ragged morphologies of PGM nanoparticles resembling sponge spicules and an Ir-rich accumulation with a rather irregular shape (Figure 3K), point to continuous in situ neoformation on the surface of ruthenian

hexaferrum grains (Figure 3). Unfortunately, the nature of PGE-bearing nanofibers could not be determined in the present study and more analytical work is necessary to understand how associated PGM nanoparticles are formed. However, considering a starting material of secondary Ru-Os-Ir alloy hosting sub-microscopic fibrous serpentine minerals, it can be speculated that (bio-)weathering of these incorporated Mg-silicate remnants drives (i) the transformation of fibrous Mg-silicates into PGE-bearing nanofibers and (ii) the formation of PGM nanoparticles of different morphologies on the surface of the grain (Figure 3).

5. Conclusions

The PGM-rich "floating chromitite" found within the highest levels of the Loma Larga ore deposit is a suitable natural laboratory which can provide important new insights helping (i) to explain PGE mobilization in the surface environment; (ii) to understand transformation processes of hypogene PGM related to supergene (bio-)weathering and (iii) to find convincing evidence for supergene PGM neoformation and processes involved.

Acknowledgments: This research has been financially supported by FEDER Funds, the Spanish project CGL2015-65824-P and the Catalan project 2014-SGR-1661, as well as by a PhD grant to TA sponsored by the Ministerio de Economia y Competitividad (Spain). The authors gratefully acknowledge the help and hospitality extended by the staff of Falcondo mine (Falcondo Glencore). Excellent technical support during EPMA sessions by Xavier Llovet and during FE-SEM sessions by Eva Prats at the Serveis Científics i Tecnòlogics (University of Barcelona) is highly appreciated. Louis Cabri and Vladimir Rudashevsky are greatly thanked for their help during installation of the HS-11 laboratory in Barcelona. Special thanks are due to the Guest Editor of the Special Issue "Mineral Deposit Genesis and Exploration" Maria Economou-Eliopoulos. Three anonymous reviewers are thanked for their constructive criticism and valuable comments that have improved the manuscript.

Author Contributions: Francisco Longo contributed materials and logistics during field work; Thomas Aiglsperger, Joaquín A. Proenza, Mercè Font-Bardia, Salvador Galí, Josep Roqué, and Sandra Baurier-Aymat performed the experiments and analyzed the data; Thomas Aiglsperger and Joaquín A. Proenza wrote the paper.

Conflicts of Interest: The authors declare no conflict of interest.

References

1. European Commission (EC). *Report on Critical Raw Materials for the EU*; Report of the Ad-Hoc Working Group in Defining Critical Raw Materials; EC: Brussels, Belgium, 2014.
2. United States Geological Survey (USGS). Mineral Commodity Summaries 2015. Available online: http://minerals.usgs.gov/minerals/pubs/commodity/platinum/mcs-2015-plati.pdf (accessed on 19 January 2016).
3. Wilde, A.; Edwards, A.; Yakubchuk, A. Unconventional deposits of Pt and Pd: A review with implications for exploration. *SEG Newsl.* **2003**, *52*, 1 and 10–18.
4. Gray, J.D.; Schorin, K.H.; Butt, C.R.M. Mineral associations of platinum and palladium in lateritic regolith, Ora Banda Sill, Western Australia. *J. Geochem. Explor.* **1996**, *57*, 245–255. [CrossRef]
5. Maier, W.D.; Barnes, S.J.; Bandyayera, D.; Livesey, T.; Li, C.; Ripley, E. Early Kibaran rift-related mafic-ultramafic magmatism in western Tanzania and Burundi: Petrogenesis and ore potential of the Kapalagulu and Musongati layered intrusions. *Lithos* **2008**, *101*, 24–53. [CrossRef]
6. Aiglsperger, T.; Proenza, J.A.; Lewis, J.F.; Labrador, M.; Svojtka, M.; Rojas-Purón, A.; Longo, F.; Ďurišová, J. Critical metals (REE, Sc, PGE) in Ni-laterites from Cuba and the Dominican Republic. *Ore Geol. Rev.* **2016**, *73*, 127–147. [CrossRef]
7. Aiglsperger, T.; Proenza, J.A.; Font-Bardia, M.; Baurier-Amat, S.; Galí, S.; Lewis, J.F.; Longo, F. Supergene neoformation of Pt-Ir-Fe-Ni alloys: Multistage grains explain nugget formation in Ni-laterites. *Miner. Depos.* **2016**. [CrossRef]
8. Aiglsperger, T.; Proenza, J.A.; Zaccarini, F.; Lewis, J.F.; Garuti, G.; Labrador, M.; Longo, F. Platinum group minerals (PGM) in the Falcondo Ni-laterite deposit, Loma Caribe peridotite (Dominican Republic). *Miner. Depos.* **2015**, *50*, 105–123. [CrossRef]
9. Reith, F.; Zammit, C.M.; Shar, S.S.; Etschmann, B.; Bottrill, R.; Southam, G.; Ta, C.; Kilburn, M.; Oberthür, T.; Ball, A.S.; et al. Biological role in the transformation of platinum-group-mineral grains. *Nat. Geosci.* **2016**, *9*, 294–298. [CrossRef]

10. Redwood, S. Gold surge Mining is booming in the Dominican Republic as investors follow the gold rush. *Min. J.* **2014**, *24*, 23–27.
11. Villanova-de-Benavent, C.; Proenza, J.A.; Galí, S.; García-Casco, A.; Tauler, E.; Lewis, J.F.; Longo, F. Garnierites and garnierites: Textures, mineralogy and geochemistry of garnierites in the Falcondo Ni-laterite deposit, Dominican Republic. *Ore Geol. Rev.* **2014**, *58*, 91–109. [CrossRef]
12. Lewis, J.F.; Draper, G.; Proenza, J.A.; Espaillat, J.; Jiménez, J. Ophiolite-related ultramafic rocks (serpentinites) in the Caribbean region: A review of their occurrence, composition, origin, emplacement and nickel laterite soils. *Geol. Acta* **2006**, *4*, 237–263.
13. Tauler, E.; Proenza, J.; Galí, S.; Lewis, J.; Labrador, M.; García-Romero, E. Ni-sepiolite-falcondite in garnierite mineralisation from the Falcondo Ni-laterite deposit, Dominican Republic. *Clay Miner.* **2009**, *44*, 435–454. [CrossRef]
14. Villanova-de-Benavent, C.; Nieto, F.; Viti, C.; Proenza, J.A.; Galí, S.; Roqué-Rosell, J. Ni-phyllosilicates (garnierites) from the Falcondo Ni-laterite deposit (Dominican Republic): Mineralogy, nanotextures, and formation mechanisms by HRTEM and AEM. *Am. Mineral.* **2016**, *101*, 1460–1473. [CrossRef]
15. Proenza, J.A.; Zaccarini, F.; Lewis, J.F.; Longo, F.; Garuti, G. Chromian spinel composition and the Platinum Group Minerals of the PGE-rich Loma Peguera chromitites, Loma Caribe peridotite, Dominican Republic. *Can. Mineral.* **2007**, *45*, 631–648. [CrossRef]
16. Baurier-Aymat, S.; Aiglsperger, T.; Proenza, J.A.; Lewis, J.F.; Longo, F. Chromian spinel composition, PGE geochemistry and PGE mineralogy of different chromitites from the Loma Caribe peridotite, Dominican Republic. In Proceedings of the 13th SGA Biennial Meeting, Nancy, France, 24–27 August 2015; Volume 3, pp. 889–892.
17. Bowin, C.O. Geology of the central Dominican Republic (a case history of part of an island arc). In *Caribbean Geological Studies*; Hess, H., Ed.; Geological Society of America: Boulder, CO, USA, 1966; Volume 98, pp. 11–84.
18. Escuder-Viruete, J.; Pérez-Estaún, A.; Contreras, F.; Joubert, M.; Weis, D.; Ullrich, T.D.; Spadea, P. Plume mantle source heterogeneity through time: Insights from the Duarte Complex, Hispaniola, northeastern Caribbean. *J. Geophys. Res.* **2007**, *112*, B04203. [CrossRef]
19. TOPAS. *General Profile and Structure Analysis for Powder Diffraction Data*, version 4.2; Bruker AXS GmbH: Karlsruhe, Germany, 2009.
20. Aiglsperger, T.; Proenza, J.A.; Galí, S.; Rius, J.; Longo, F.; Domènech, C. The supergene origin of Ruthenian Hexaferrum in Ni-laterites. *Terra Nova* **2016**, accepted.
21. Konishi, Y.; Ohno, K.; Saitoh, N.; Nomura, T.; Nagamine, S.; Hishida, H.; Takahashi, Y.; Uruga, T. Bioreductive deposition of platinum nanoparticles on the bacterium Shewanella algae. *J. Biotechnol.* **2007**, *128*, 648–653. [CrossRef] [PubMed]
22. Mochalov, A.G.; Dmitrenko, G.G.; Rudashevsky, N.S.; Zhernovsky, I.V.; Boldyreva, M.M. Hexaferrum (Fe,Ru), (Fe,Os), (Fe,Ir)—A new mineral. *Zap Vseross Miner. Obshch* **1998**, *127*, 41–51. (In Russian)
23. Urashima, Y.; Wakabayashi, T.; Masaki, T.; Terasaki, Y. Ruthenium, a new mineral from Horokanai, Hokkaldo, Japan. *Miner. J. (Jpn.)* **1974**, *7*, 438–444. [CrossRef]
24. Swanson, H.E.; Fuyat, R.K.; Ugrinic, G.M. Standard X-ray diffraction powder patterns. *Natl. Bur. Stand. (U.S.)* **1955**, *IV*, 8.
25. McDonald, A.M.; Proenza, J.A.; Zaccarini, Z.; Rudashevsky, N.S.; Cabri, L.J.; Stanley, C.J.; Rudashevsky, V.N.; Melgarejo, J.C.; Lewis, J.F.; Longo, F. Garutiite, (Ni,Fe,Ir), a new hexagonal polymorph of native Ni from Loma Peguera, Dominican Republic. *Eur. J. Mineral.* **2010**, *22*, 293–304. [CrossRef]
26. Garuti, G.; Zaccarini, F. In situ alteration of platinum-group minerals at low temperature: Evidence from serpentinized and weathered chromitite of the Vourinos complex, Greece. *Can. Miner.* **1997**, *35*, 611–626.
27. Uysal, I.; Zaccarini, F.; Sadiklar, M.B.; Bernhardt, H.-J.M.; Bigi, S.; Garuti, G. Occurrence of rare Ru-Fe-Os-Ir–oxide and associated Platinum-group minerals (PGM) in the chromitite of Mugla ophiolite, SW-Turkey. *Neues Jahrb. Mineral. (Abh.)* **2009**, *185*, 323–333. [CrossRef]